

Experimentally verifying anti-Kibble-Zurek behavior in a quantum system under noisy control field

Ming-Zhong Ai, Ran He, Zhong-Hua Qian, Jin-Ming Cui,* Yun-Feng Huang,† Chuan-Feng Li,‡ and Guang-Can Guo

CAS Key Laboratory of Quantum Information, University of Science and

Technology of China, Hefei, 230026, People's Republic of China. and

CAS Center For Excellence in Quantum Information and Quantum Physics,

University of Science and Technology of China, Hefei, 230026, People's Republic of China.

Kibble-Zurek mechanism (KZM) is a very significant framework which could in principle describe phase transition phenomenon in any system with required symmetry properties. Anti-KZ behavior is a special case of KZM when the quench dynamics couple to a dissipative thermal bath, whereby slower driving results in more topological defects. In this work, we for the first time experimentally demonstrate anti-KZ behavior under noisy control field in three kinds of quantum phase transition protocols using a single trapped $^{171}\text{Yb}^+$ ion. The density of defects is studied as a function of the quench time and the noise strength. We experimentally verify that the optimal quench time to minimize excitations scales as a universal power law of the noise strength. Our research set a stage for quantum simulation of such anti-KZ behavior in two-level systems and reveal the limitations of the adiabatic protocols such as quantum annealing.

Kibble-Zurek mechanism (KZM), which originally proposed to describe early-universe phase transition by Kibble and Zurek [1, 2], provides an elegant theoretical framework for exploring the critical dynamics of phase transition [3]. Its central prediction is that the density of topological defects n_0 , formed when a system is driven through a critical point in a time scale τ , follows a universal power law as a function of quench time: $n_0 \propto \tau^{-\beta}$. The power-law exponent $\beta = d\nu/(1 + z\nu) > 0$ is determined by the dimensionality of the system d , equilibrium correlation-length ν and dynamic critical exponents z respectively [4]. Notably, in the quantum domain, the KZM provides useful heuristic for the preparation of ground-state phases of matter in quantum simulation as well as for adiabatic quantum computation [5]. Although the KZM has many important implications, its experimental verification still calls for further studies. For classical continuous phase transitions, many systems have verified this mechanism, such as cold atomic gases [6], ion crystals [7, 8], and superconductors [9]. Meanwhile for quantum phase transitions, which are accomplished by varying a parameter in the Hamiltonian in order to tune between different quantum phases, its experimental verification are still scarce due to the difficulty of exactly controlling driven parameters [10–14]. And it had been performed only in few platforms through quantum simulators [15–17].

While the KZM is believed to be broadly applicable, a conflicting observation has been reported in the study of ferroelectric phase transition: slower quenches generate more topological defects when approaching the adiabatic limit [18]. Opposited to that predicted by standard KZM, this counterintuitive phenomenon is termed

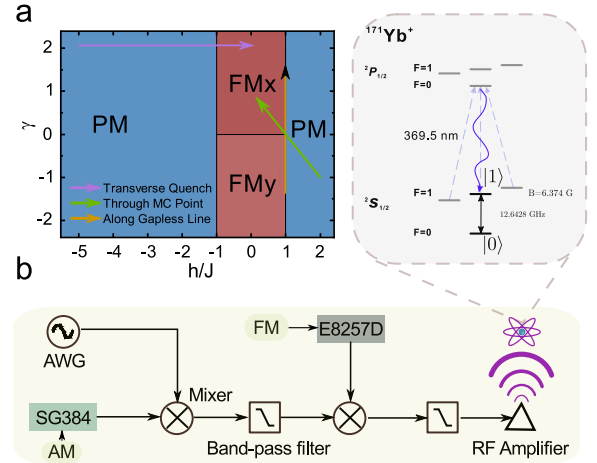


Figure 1. (color online). Phase diagram of three quantum phase transition protocols and the schematic diagram of the experimental device. (a) The phase diagram is divided into paramagnetic phase and ferromagnetic phase which are denoted by PM and FM respectively. These two phase is separated by the parameter $h/J = \pm 1$ in our $\gamma - hJ$ frame. The middle ferromagnetic phase is also divided into two parts by the line $\gamma = 0$, which ordering along x and y directions. The three lines with arrow represent three quench protocols explained in legend. (b) The microwave used in our experiments is generated by a mixing wave scheme. The illustration in (a) is the energy level diagram of $^{171}\text{Yb}^+$ ion.

as anti-Kibble-Zurek (anti-KZ) dynamics. Considerable attention has been devoted to the anti-KZ mechanism in the last decade. The universal properties of quantum quenches of a quantum system coupling to thermal dissipation simulated using transverse field Ising model is theoretically studied in [19, 20], which exhibits anti-KZ behavior. Meanwhile, Adolfo et al. show a thermally isolated system driven across a quantum phase transition under a noisy control field also exhibits anti-KZ behavior, whereby slower driving results in higher density of

* jmcui@ustc.edu.cn

† hyf@ustc.edu.cn

‡ cfli@ustc.edu.cn

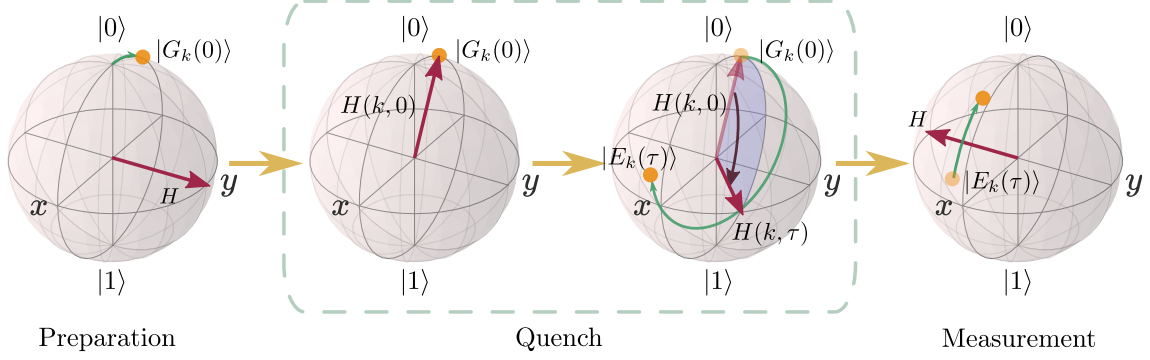


Figure 2. (color online). Scheme to measure the excitation probability. The quantum critical dynamics of the one-dimensional transverse-field XY chain model is detected by measuring corresponding Landau-Zener crossings governing the dynamics in each mode. For each mode, a typical process to measure the excitation probability is preparation, quench and measurement.

defects. In order to explore whether the anti-KZ behavior can exhibit in other quantum spin models with different scaling exponents under noise control fields, dynamics of a transverse-field XY chain driven across quantum critical points under noisy control fields is studied in [21]. And this work also proposes an experimentally feasible scheme to test the predicted anti-KZ behavior.

In this paper, we for the first time experimentally verified anti-KZ mechanism in quantum phase transition with three different scaling exponents using the two level system (TLS) with Landau-Zener (LZ) crossings in a trapped $^{171}\text{Yb}^+$ ion. Different scaling exponents are realized through quenching the boundary line between paramagnetic and ferromagnetic phase, quenching across the isolated multicritical (MC) point and quenching along the gapless line, respectively [22–24]. Utilizing built-in Gaussian noise of the microwave signal source, we experimentally investigate the density of topological defects as a function of the quench time and the strength of Gaussian noise. The results agree well with the theoretical expectation in [21], which the optimal quench time to minimize defects scales as a universal power law of the noise strength in all three protocols.

The Hamiltonian of a spin-1/2 quantum XY chain under a uniform transverse field is given by:

$$H_1 = -\frac{1}{2} \sum_{n=1}^N (J_x \sigma_n^x \sigma_{n+1}^x + J_y \sigma_n^y \sigma_{n+1}^y + h \sigma_n^z), \quad (1)$$

in which we consider only the nearest neighbor interaction. The variable N counts the number of spins, h measures the strength of the transverse field, J_x and J_y represent the anisotropy interactions along x and y spin directions respectively. Symbols σ_n^i are Pauli matrices ($i = x, y, z$) for the n th spin. For the purpose of convenience, we set $J = J_x + J_y$, $\gamma = (J_x - J_y)/J$, then the Hamiltonian can be rewritten as

$$H_2 = -\frac{J}{2} \sum_{n=1}^N [(1 + \gamma) \sigma_n^x \sigma_{n+1}^x + (1 + \gamma) \sigma_n^y \sigma_{n+1}^y] - h \sum_{n=1}^N \sigma_n^z. \quad (2)$$

According to Jordan-Wigner (J-W) transformation, which can transform a spin-1/2 system to a system of spinless free fermions [25–27], previous transverse field XY chain Hamiltonian can be transformed to the fermionic form:

$$H_3 = -J \sum_{l=1}^N [(c_l^\dagger c_{l+1} + c_{l+1}^\dagger c_l) + \gamma (c_l^\dagger c_{l+1}^\dagger + c_{l+1} c_l)] - h \sum_{l=1}^N (2c_l^\dagger c_l - 1), \quad (3)$$

in which c_l is obtained by J-W transformation: $\sigma_n^\pm = \exp(\pm i\pi \sum_{m=1}^{n-1} c_m^\dagger c_m) c_n$ and $\sigma_n^z = 2c_n^\dagger c_n - 1$. Under the periodic boundary condition $\sigma_{N+1}^\alpha = \sigma_1^\alpha$ and the Fourier transformation with $c_n = \frac{e^{-i\pi/4}}{\sqrt{N}} \sum_{k \in (-\pi, \pi]} (e^{ikn} c_k)$, this Hamiltonian can be decoupled into a sum of independent terms $H_3 = \sum_{k \in [0, \pi]} H_m(k)$, where the Hamiltonian density $H_m(k)$ in pseudomomentum space can be written as:

$$H_m(k) = -2[\sigma_z(J \cos k + h) + \sigma_x(J \gamma \sin k)]. \quad (4)$$

The evolution of the generic state $\psi_k(t)$ is governed by Schrodinger equation $i \frac{d}{dt} |\psi_k(t)\rangle = H_m(k, t) |\psi_k(t)\rangle$. This reduces the quantum many-body transverse field XY chain Hamiltonian to an array of decoupled single spin-1/2 Hamiltonians, which could be simulated utilizing a two level system with well-designed Landau-Zener crossings experimentally, such as a trapped ion qubit.

For the convenience of experimentally demonstration, variation of one parameter in $H_m(k)$ is considered. The

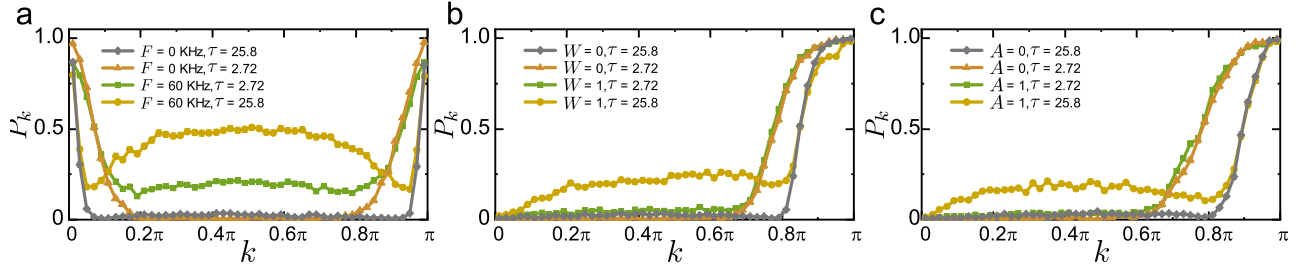


Figure 3. (color online). The probability of excited state p_k as a function of k for all three quench protocols. (a) Transverse quench protocol. The ginger and green represent probability under noisy control field with frequency deviation 60 KHz. The white Gaussian noise causes excitation near $\pi/2$ compared with noise-free case denoted by brown and gray dots. (b) and (c) are quenching along gapless line and through MC point protocols respectively with different noise coefficient A . For each point, the experiment is repeated 1000 times and the error bars indicate a standard deviation.

phase diagram of the transverse-field XY chain, which is spanned by parameters h/J and γ , is divided into four parts: the quantum paramagnetic phase PM and two ferromagnetic long-ranged phases ordering along x and y directions denoted by FMx and FMy respectively as shown in Fig. 1(b). The definition of the density of defects in this transverse field XY chain after quench is similar to the case for the Ising model [28–30], which could be denoted by:

$$n_W = \frac{1}{N_k} \sum_{k \in [0, \pi]} p_k, \quad (5)$$

where N_k is the number of k -modes used in the summation of Hamiltonian $H_m(k)$, and p_k is the probability measured in the excited state $|E_k(\tau)\rangle$ after evolution driven under the k th-mode Hamiltonian from $|G_k(0)\rangle$. Notably, $\{|G_k(t)\rangle, |E_k(t)\rangle\}$ is the basis of adiabatic instantaneous eigenstate of $H_m(k)$.

In order to observe anti-KZ phenomenon, driving with noisy control fields in the simulation is considered. White Gaussian noise is a good approximation to ubiquitous colored noise with exponentially decaying correlations, therefore the noise term $\eta(t)$ is set as white Gaussian noise with zero mean and second moment $\eta(t)\eta(t') = W^2\delta(t-t')$. Here W^2 represents the strength of the noise fluctuation. We add this noise term to quench parameter in the form of $f(t) = f^{(0)}(t) + \eta(t)$, where $f^{(0)}(t) \propto t/\tau$ is the perfect control parameter linearly varying in time with quench time τ .

Our experiments are performed using a trapped $^{171}\text{Yb}^+$ ion in needle trap with the setup simplified shown in Fig. 1(c). Two hyperfine levels of $^{171}\text{Yb}^+$ ion in the $S_{1/2}$ ground state, which means $|^2S_{1/2}, F=0, m_F=0\rangle$ and $|^2S_{1/2}, F=1, m_F=0\rangle$, are encoded to $|0\rangle$ and $|1\rangle$ respectively. The microwave used to drive this ion qubit is generated through mixing twice. A microwave signal around 200 MHz generated from a two channel Arbitrary Waveform Generator (AWG) is mixed with a 3.0 GHz microwave generated from a RF signal generator (SG384, Stanford Research Systems). This mixed signal is mixed

again with a 9.44 GHz microwave generated from a Analog Signal Generator (E8257D, Agilent) to obtain an arbitrary microwave near 12.64 GHz, and then this signal is amplified to about 2 W and irradiated to the trapped ion by a horn antenna. In all of our experiments, the Rabi time is set to 100 μs and all expressions of τ in the following text represent multiples of the Rabi time.

We first consider the transverse quench, in which case only the parameter $h(t)$ is time-dependent, as shown in Fig. 1(b). To simulate the quench dynamics under noise fluctuation, white Gaussian noise $\eta(t)$ is added to the time-dependent quench parameter $h(t)$ as described above. The Hamiltonian of Equ. 4 can be rewritten as:

$$H_m^{(1)}(k, t) = -2[(J_x + J_y)\cos k + h(t)]\sigma_z - 2[(J_x - J_y)\sin k]\sigma_x - 2\eta(t)\sigma_z. \quad (6)$$

This Hamiltonian can be transformed into standard LZ model $H_{LZ}(k, t) = -\frac{1}{2}(\sigma_x + \nu_{LZ}t_{LZ}\sigma_z)$ using the substitutions $\nu_{LZ} = \nu_h/(2J\gamma\sin k)^2$, $t_{LZ} = 4J\gamma\sin k(t + J\cos k/\nu_h)$, in which $h(t) = \nu_h t$ and ν_h is the quench velocity. The standard LZ model could be simulated through a trapped ion qubit as described in Ref. [16]. We first drive the qubit to the groundstate $|G_k(0)\rangle$ of Hamiltonian $H_m^{(1)}(k, 0)$, which is followed by evolution over time controlled by this Hamiltonian. The quench parameter $h(t)$ varies linearly from -5 to 0 with entire quench time τ while the other two independent parameters are fixed as $J_x = 1$ and $J_y = -1/3$ in the evolution. Finally the state is driven again to the basis $\{|0\rangle, |1\rangle\}$, which is the reverse process of the first driven, to measure the population probability p_k of the excited state $|E_k(\tau)\rangle$ by fluorescence detection scheme. The white Gaussian noise in this quench protocol is generated through frequency modulation (FM) the microwave generated by SG384 utilizing built-in noise source (the detailed form of this noise is described in Supplemental Material). Different noise strength are realized through varying frequency deviation F in FM. We decompose the Hamiltonian $H(t)$ into 50 independent terms $H_m(k, t)$ in all three protocols, and the parameter k is sampled 50 times equidistantly

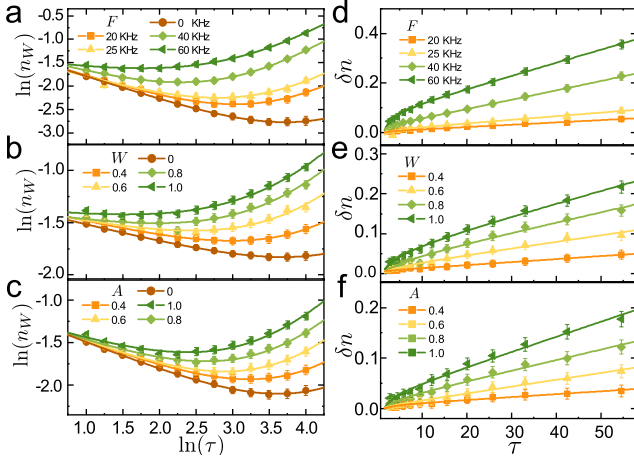


Figure 4. (color online). The anti-KZ behavior of defect productions in three quench protocols. The defects density $\ln(n_W)$ as a function of quench time $\ln(\tau)$ are shown in (a), (b) and (c), in which the defects rise with the increase of strength of noise in the limitation of long quench time. The corresponding noise-induced defect density $\delta n = n_W - n_0$ in these three cases are shown in (d), (e) and (f). These picture's layout are arrange in the order of transverse quench, anisotropic quench across the multicritical point and quench along the gapless line. For each point, the experiment is repeated 1000 times and the error bars indicate a standard deviation.

from 0 to π . The final population probability p_k as a function of k under different noise strength and quench time are shown in Fig. 3(a). As a result, the white Gaussian noise causes bulge around $k = \pi/2$, which is the reason of addition of the density of defects in this quench process. And the stronger the noise is, the more defects would be generated.

We proceed to consider the second quench protocol, the anisotropic quench across the multicritical point, as shown in Fig. 1(b). The Hamiltonian for each k -mode in this case can be rewritten as:

$$H_m^{(2)}(k, t) = -2\{[J_x(t) + J_y]\cos(k) + h\}\sigma_z - 2[(J_x(t) - J_y)\sin(k)]\sigma_x - 2\eta(t)[(\sin k)\sigma_x + (\cos k)\sigma_z] \quad (7)$$

with time-dependent quench parameter $J_x(t)$ ramping from 0 to 3. The Hamiltonian $H_m^{(2)}(k, t)$ can be transformed into standard LZ model using the substitutions $\nu_{LZ} = \nu_x/[2(J_y \sin 2k + h \sin k)]^2$, $t_{LZ} = 4(J_y \sin 2k + h \sin k) \times [t + (J_y \cos 2k + h \cos k)/\nu_x]$. Similar to the first protocol, we fix $h = 2$ and $J_y = 1$ in all experiments of this protocol and under this condition, the system is initially in the PM phase and then driven through the multicritical point into the FMx phase. The noise used in this quench protocol is induced through frequency modulation (FM) SG384 and amplitude modulation (AM) E8257D synchronously utilizing built-in Gaussian noise respectively. Different noise strength is real-

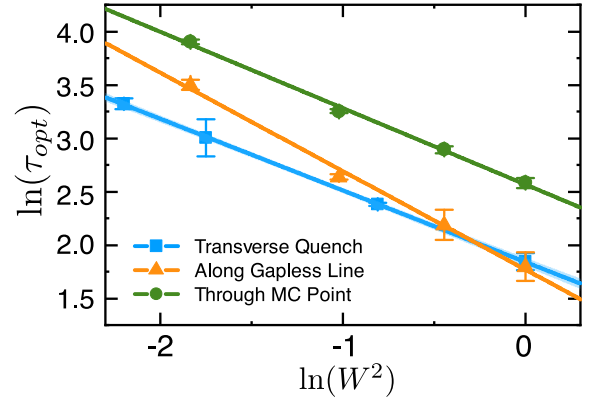


Figure 5. (color online). The fitting of logarithm of optimal quench time $\ln(\tau_{opt})$ as a function of logarithm of the square of noise strength $\ln(W^2)$ gives $\ln(\tau_{opt}) \propto \alpha_{fit} \ln(W^2)$. The fitting parameters of these three quench protocols are: $\alpha_{fit} = -0.67 \pm 0.0065$ for the transverse quench, which is close to analytical result $\alpha = -0.67$; $\alpha_{fit} = -0.92 \pm 0.046$ for the quench through the multicritical point with $\alpha = -0.86$; $\alpha_{fit} = -0.71 \pm 0.027$ for the quench along gapless line with $\alpha = -0.75$. The error bars indicate a standard deviation.

ized by changing frequency deviation F and modulation depth A proportionally. For convention, we represent the noise strength W through percentage, which in AM is the modulation depth $W = A$ and in FM is the ratio $W = F/60\text{KHz}$. The probabilities p_k measured in excited state as a function of k with different noise strength and quench time are shown in Fig. 3(b).

For the last quench protocol along the gapless line, the Hamiltonian for each k -mode is:

$$H_m^{(3)}(k, t) = -2[(J \cos k + h)\sigma_z + J\gamma(t)\sin k\sigma_x] - 2\eta(t)J\sin k\sigma_x, \quad (8)$$

in which the time-dependent parameter $\gamma(t)$ ramping from -2 to 2 while the other parameters are fixed as $h = 1$ and $J = J_x + J_y = 1$. This Hamiltonian could be transformed into standard LZ model using the substitutions $\nu_{LZ} = \nu_\gamma \sin k / [2(\cos k + 1)]^2$, $t_{LZ} = -4(\cos k + 1)t$. The noise is induced through amplitude modulation (AM) the microwave source E8257D utilizing built-in Gaussian noise. Figure 3(c) shows the probabilities p_k measured in excited state as a function of k with different noise strength and quench time.

The defects density exhibits anti-KZ behavior in all of these three quench protocols when the noise presents, which makes it possible to find a optimal quench time τ_{opt} to minimize the defects density. As the defects density under the control of noise $n_W \approx r_W \tau + c\tau^{-\beta}$ where the prefactor c is predicted by KZM and r_W characterizes the strength of the noise, we can define

$$\delta n = n_W - n_0 \approx r_W \tau + c\tau^{-\beta} - (r_0 \tau + c\tau^{-\beta}) = \delta r \tau. \quad (9)$$

to represent the defect density induced by noise in control field. The results are shown in Figure 4. Now that the parameter r_W represents the productivity of defects where the noise appeared in the control field, we can remove the system noise by subtract r_0 from r_W to indicate the efficiency of defects induced by noise in control field, in which r_0 is the fitting parameter in noise-free driving field in these protocols respectively. We use the expression $n_W \approx \delta r \tau + c \tau^{-\beta}$ to find the optimal quench time τ_{opt} to minimize n_W . And as illustrated in Fig. 5, the optimal quench time to minimize defects scales as a power law of the noise strength W in all of these three protocols. Linear fitting $\ln(\tau_{opt})$ as a function of $\ln(W^2)$ gives $\ln(\tau_{opt}) \propto \alpha_{fit} \ln(W^2)$ where the fitting parameters for the three cases agree well with analytical result: $\alpha_{fit} = -0.67 \pm 0.0065$ for the transverse quench with $\alpha = -2/3 = 0.67$; $\alpha_{fit} = -0.92 \pm 0.046$ for the quench through the multicritical point with $\alpha = -6/7 = -0.86$; $\alpha_{fit} = -0.71 \pm 0.027$ for the quench along gapless line with $\alpha = -3/4 = -0.75$ [23, 31, 32].

In summary, we for the first time experimentally studied the anti-KZ behavior in three quantum phase transition protocols under white Gaussian noisy control field

using a single trapped ion. The experimental results can be used as a powerful evidence for anti-KZ phenomenon. We also show the optimal quench time to minimize defects density τ_{opt} scales as a universal power law of the noise strength W for all of these three cases, which may inspire the limitations of adiabatic protocols such as quantum annealing.

ACKNOWLEDGMENTS

This work was supported by the National Key Research and Development Program of China (Nos. 2017YFA0304100, 2016YFA0302700), the National Natural Science Foundation of China (Nos. 11874343, 61327901, 11774335, 11474270, 11734015, 11874343), Key Research Program of Frontier Sciences, CAS (No. QYZDY-SSW-SLH003), the Fundamental Research Funds for the Central Universities (Nos. WK2470000026, WK2470000018), An-hui Initiative in Quantum Information Technologies (AHY020100, AHY070000), the National Program for Support of Topnotch Young Professionals (Grant No. BB2470000005).

-
- [1] T. W. Kibble, Journal of Physics A: Mathematical and General **9**, 1387 (1976).
 - [2] W. H. Zurek, Nature **317**, 505 (1985).
 - [3] A. D. CAMPO and W. H. Zurek, in *Symmetry and Fundamental Physics: Tom Kibble at 80* (World Scientific, 2014) pp. 31–87.
 - [4] A. Dutta, A. Rahmani, and A. del Campo, Physical review letters **117**, 080402 (2016).
 - [5] S. Suzuki, in *Quantum Quenching, Annealing and Computation* (Springer, 2010) pp. 115–143.
 - [6] N. Navon, A. L. Gaunt, R. P. Smith, and Z. Hadzibabic, Science **347**, 167 (2015).
 - [7] S. Ulm, J. Roßnagel, G. Jacob, C. Degünther, S. Dawkins, U. Poschinger, R. Nigmatullin, A. Retzker, M. Plenio, F. Schmidt-Kaler, *et al.*, Nature communications **4**, 2290 (2013).
 - [8] K. Pyka, J. Keller, H. Partner, R. Nigmatullin, T. Burgermeister, D. Meier, K. Kuhlmann, A. Retzker, M. B. Plenio, W. Zurek, *et al.*, Nature communications **4**, 2291 (2013).
 - [9] R. Monaco, R. Rivers, and J. Mygind, *The Dynamics of Spontaneous Fluxon formation in Annular Josephson Tunnel Junctions*, Tech. Rep. (2001).
 - [10] D. Chen, M. White, C. Borries, and B. DeMarco, Physical Review Letters **106**, 235304 (2011).
 - [11] S. Braun, M. Friesdorf, S. S. Hodgman, M. Schreiber, J. P. Ronzheimer, A. Riera, M. Del Rey, I. Bloch, J. Eisert, and U. Schneider, Proceedings of the National Academy of Sciences **112**, 3641 (2015).
 - [12] M. Anquez, B. Robbins, H. Bharath, M. Boguslawski, T. Hoang, and M. Chapman, Physical review letters **116**, 155301 (2016).
 - [13] B. Gardas, J. Dziarmaga, W. H. Zurek, and M. Zwolak, Scientific reports **8**, 4539 (2018).
 - [14] A. Keesling, A. Omran, H. Levine, H. Bernien, H. Pichler, S. Choi, R. Samajdar, S. Schwartz, P. Silvi, S. Sachdev, *et al.*, arXiv preprint arXiv:1809.05540 (2018).
 - [15] X.-Y. Xu, Y.-J. Han, K. Sun, J.-S. Xu, J.-S. Tang, C.-F. Li, and G.-C. Guo, Physical review letters **112**, 035701 (2014).
 - [16] J. Cui, Sci Rep. **6**, 33381 (2016).
 - [17] M. Gong, X. Wen, and G. Sun, Sci. Rep. **6**, 22667 (2016).
 - [18] S. M. Griffin, M. Lilienblum, K. T. Delaney, Y. Kumagai, M. Fiebig, and N. A. Spaldin, Physical Review X **2**, 041022 (2012).
 - [19] D. Patane, A. Silva, L. Amico, R. Fazio, and G. E. Santoro, Physical review letters **101**, 175701 (2008).
 - [20] P. Nalbach, S. Vishveshwara, and A. A. Clerk, Physical Review B **92**, 014306 (2015).
 - [21] Z.-P. Gao, D.-W. Zhang, Y. Yu, and S.-L. Zhu, Physical Review B **95**, 224303 (2017).
 - [22] V. Mukherjee, Phys. Rev. B **76**, 174303 (2007).
 - [23] U. Divakaran, V. Mukherjee, A. Dutta, and D. Sen, Journal of Statistical Mechanics: Theory and Experiment **2009**, P02007 (2009).
 - [24] U. Divakaran, Phys. Rev. B **78**, 144301 (2008).
 - [25] E. Lieb, T. Schultz, and D. Mattis, Annals of Physics **16**, 407 (1961).
 - [26] J. Bunder, Phys. Rev. B **60**, 344 (1999).
 - [27] T. Caneva, R. Fazio, and G. E. Santoro, Physical Review B **76**, 144427 (2007).
 - [28] J. Dziarmaga, Advances in Physics **59**, 1063 (2010).
 - [29] J. Dziarmaga, Physical review letters **95**, 245701 (2005).
 - [30] W. H. Zurek, U. Dorner, and P. Zoller, Physical review letters **95**, 105701 (2005).
 - [31] V. Mukherjee, U. Divakaran, A. Dutta, and D. Sen, Physical Review B **76**, 174303 (2007).

- [32] U. Divakaran, A. Dutta, and D. Sen, Physical Review B **78**, 144301 (2008).